Computation of the Relationships of X-ray to Radio Luminosities of a Sample of Starburst Galaxies

Maha M. Zamal*, Al Najm M. N.

Department of Astronomy and Space, College of Science, University of Baghdad, Baghdad, Iraq

Abstract

The goal of this research is to better understand the physical features of starburst galaxies. Radio and X-ray observations are good for exploring the stuff within the central regions of galaxies. A galaxy that is undergoing a strong star formation, usually in its central area, is known as a starburst galaxy. This paper provides the results of a statistical analysis of a sample of starburst galaxies. The data used in this research have been collected from NASA Extragalactic Database (NED), and HYPERLEDA. Those data have been used to examine possible luminosity correlations of X-ray to a radio of a sample of starburst galaxies. In this research, statistical software, known as statistic-win-program, has been used to investigate if there is a luminosity correlation between multiple-wavelength bands. The results of the statistical analysis conclude that there is a good correlation between X-ray luminosity and radio luminosity at 1.4GHz where the partial correlation coefficient is ($R \approx 0.53$) and slope (0.6 ± 0.12). There is also a good correlation between X-ray luminosity and radio luminosity at 5GHz with a good partial correlation coefficient ($R \approx 0.65$) and slope (0.77 ± 0.11). There are good positive relationships between radio luminosity at (1.4GHz, 5GHz) with infrared and far-infrared luminosities (Log $L_{1.4GHz}$ α log $L_{FIR}^{0.89 \pm 0.04}$ α Log $L_{IR}^{0.9 \pm 0.03}$) with a very strong correlation equal to R=0.9 (Log L_{5GHz} α Log $L_{FIR}^{0.79 \pm 0.05}$ α Log $L_{IR}^{0.81 \pm 0.05}$) with strong correlation R=0.8 both with very high probability level $p \approx 10^{-7}$. One of the closest and most ubiquitous correlations known among the global features of local star formation and starburst galaxies is the link between far-infrared (FIR) and radio emission.

Keywords: Galaxies, Active galaxies, Starburst, X-ray galaxies, Radio continuum statistics.

<div dir="rtl">

حساب العلاقات بين الضيائيات من الأشعة السينية الى الراديوية لعينة من المجرات ذات الانفجارات النجمية

مها محمد زامل* ، محمد ناجي ال نجم

قسم الفلك والفضاء، كلية العلوم، جامعة بغداد ، بغداد ، العراق

</div>

*Email: maha.mohammed1207m@sc.uobaghdad.edu.iq

الخلاصه

الهدف من هذا البحث هو فهم أفضل المميزات الفيزيائية للمجرات ذات الانفجارات النجمية. تعد الارصاد الراديوية والأشعة السينية ادوات جيدة لاستكشاف التأثيرات داخل المنطقة المركزية المجرة. تعرف المجرة التي تمر بانفجارا قصيرا لتشكيل نجمي قوي, عادة في منطقتها المركزية, باسم المجرة ذات انفجار نجمي. تقدم هذه الورقة البحثية نتائج تحليل إحصائي لعينة من مجرات الانفجار النجمي. تم جمع البيانات المستخدمة في هذا البحث من قواعد البيانات التالية: (NED) NASA Extragalactic Database و HYPERLEDA.تم استخدم هذه البيانات لدراسة ارتباطات الضيائيات المحتملة من الأشعة السينية الى الراديوية لعينة من المجرات ذات الانفجارات النجمية. في هذا البحث ، تم استخدام تطبيقا إحصائيا يعرف باسم (statistic−win−program) لمعرفة فيما إذا كان هناك ارتباطات بين الضيائيات لنطاقات متعددة الاطوال الموجية. خلصت نتائج التحليل الإحصائي الى وجود علاقة ارتباط معنوية بين ضيائية الأشعة السينية والضيائية الراديوية عند تردد 1.4 جيجاهرتز حيث كان معامل الارتباط الجزئي ($R \approx 0.53$) و الميل (0.6 ± 0.12). هناك أيضا علاقة معنوية بين ضيائية الأشعة السينية والضيائية الراديوية عند تردد 5 جيجاهرتز مع معامل ارتباط جزئي جيد ($R \approx 0.65$) وميل (0.77 ± 0.11). هناك علاقات ارتباط إيجابية جيدة بين اللمعان الراديوي عند (1.4 جيجا هرتز ، 5 جيجا هرتز) مع لمعان الأشعة تحت الحمراء والأشعة تحت الحمراء البعيدة. ($\text{Log } L_{1.4GHz} \, \alpha \, \log$ $L_{FIR}^{0.89\pm0.04} \, \alpha \, \text{Log } L_{IR}^{0.9\pm0.03}$ مع ارتباط قوي جدا يساوي R=0.9 و $\text{Log } L_{5GHz} \, \alpha \, \text{Log } L_{FIR}^{0.79\pm0.05}$) ($\alpha \, \text{Log } L_{IR}^{0.81\pm0.05}$ مع ارتباط قوي $R \approx 0.8$ كلاهما مع مستوى احتمالية عالي جدا $p \approx 10^{-7}$. احد أقرب الارتباطات وأكثرها انتشارا المعروفة بين السمات الشاملة لتكوين النجوم المحلية والمجرات ذات الانفجارات النجمية هي الارتباط بين الأشعة تحت الحمراء البعيدة (FIR) والانبعاثات الراديوية.

1. Introduction

Massive stars are the source of power for starbursts. Massive stars ($M_{starbursts} \geq 10 \, M_\odot$) produce ultraviolet resonance transitions by emitting photons with energy of tens of eV that are absorbed and re-emitted in their stellar winds. The stellar wind, on the other hand, is optically thin to most ultraviolet photons, which can travel tens of kilometers from the star before being absorbed and photoionizing the interstellar medium. The ionized gas is then cooled down using an emission line spectrum. In essence, this is a starburst galaxy's spectral dichotomy picture: a nebular emission line spectrum at optical wavelengths and an absorption-line spectrum at wavelengths shorter than the Balmer jump [1]. Starburst galaxies are objects in which star formation and associated processes dominate the total energy. They have a size range of 100 pc to 1000 pc, and H_α luminosity of 10^{40} erg/s to 10^{42} erg/s. As a result, the nebula requires an ionizing photon brightness of between 10^{52} and 10^{54} photons per second, which is supplied by a stellar cluster containing thousands of young massive stars. This concept encompasses a wide spectrum of galaxies, including blue compact dwarfs, HII galaxies, nuclear starbursts, and ultraluminous IRAS starbursts, among others. Typical bolometric luminosities range from 10^{40} erg/s to 10^{45} erg/s, with the lowest limit corresponding to super-star cluster luminosity and the greatest limit corresponding to infrared-luminous galaxies. The pace of star formation is significant (10-100 and up to 1000 $M_\odot$/yr in some ultraluminous infrared galaxies) that the present gas supply can only fuel the starburst for a fraction of the universe's history (few 10^8 yr) [2].

In earlier research, the ROSAT All Survey was cross-correlated with a sample of 14708 extragalactic IRAS sources taken from the point source database by statistical classification. The X-ray brilliant spirals are starbursts with steep spectra, which makes them simpler to identify by ROSAT. They discovered a positive link between X-ray luminosity, IR, and optical

luminosities, with the steepest correlation for Seyfert galaxies [3]. In addition, [4] discovered that barred galaxies have lower overall FIR luminosity than unbarred galaxies in a volume-limited sample. Other researchers confirmed that IR bright barred galaxies have much larger FIR-optical and S_{25}/S_{12} ratios than unbarred galaxies, with the effect being particularly noticeable in the IR hues. They further showed that the influence of bars on the SFR was linked to relative IR luminosity and that it could only be seen in galaxies with $L_{FIR}/L_B \geq 1/3$ [5]. Moreover, [6] offered the results of a statistical study of AGNs chosen from an RBSC-NVSS sample as the strongest X-ray sources. They discovered that the slopes of the L_X-L_B relations were flat for Seyfert galaxies, including the presence of components unrelated to X-ray. [7] presented a statistical analysis of samples of bright X-ray galaxies with active galactic nuclei (Seyferts1, Seyferts2, and Quasars) from the ROSAT Bright Source Catalogue (RBSC) and the NRAO VLA Sky Survey (NVSS). Multi-wavelength observations in the radio (1.4GHz), blue optical (4400 A^0), and X-ray (0.1-2.4) keV bands were investigated. The results of their statistical analysis showed that there was a strong correlation between the quantities (L_{X-ray} - D and $L_{1.4}$ - D correlations), and the slopes of the relation (L_B-D) were flatter than the slope of 0.5 expected for cosmologically nearby objects, whereas for Seyfert2 type galaxies, they found that there was a very strong correlation between relation (L_{X-ray} - D and L_B - D), indicating that in comparison to Seyfert1, Seyfert2 had active components unrelated to radio emission. They also discovered that the Seyfert 1 and 2 galaxies had a strong linear relationship between (L_{X-ray} - D), which could be due to the presence of extremely high X-ray emission in broad emission lines in their nuclei. The IRAF ISOPHOTE ELLIPSE job with Griz-Filters was used to investigate the morphological and photometric properties of two lenticular galaxies (NGC 2577, NGC 4310). The Sloan Digital Sky Survey (SDSS) provided observations, which are now available in the Data Release (DR14). The SDSS pipeline was used to reduce the data in all of the photos (bias and flat field). Although the disk position angle, ellipticity, and inclination of the galaxies were investigated, the surface photometric investigations such as total magnitude, isophotal contour maps, surface brightness profiles, and a bulge/disk decomposition of the photos of the galaxies were done by[8]. Eventually, [9] used their data from Chandra XMM-Newton and other wavebands to analyze the X-ray emission for a sample of young radio AGNs. For VLBI radio-core, they discovered strong correlations between X-ray luminosity in (2-10) KeV and radio luminosities L_R at 5GHz. In the current study, we use data from the following sources in this inquiry, the first source is NASA Extragalactic Database (NED), and the second is HYPERLEDA. Those data are used to examine possible luminosity correlations of X-ray to a radio of a sample of starburst galaxies. This article is organized as follows: The second section describes the mathematical procedure utilized in this project to produce the form used in mathematical analysis, as well as the derivation of the parameters used in this analysis. The third section presents the findings of the statistical analysis that have been carried out in this research. Finally, the work's conclusion will be summarized in section four.

2. The data utilized and estimated parameters in the sample.

A sample of starburst galaxies was selected from papers [10] [11] [12] [13] [14] [15] [16] [17] [18]. Based on the NASA/IPAC Extra-Galactic Database (NED), selected available data such as redshift(z), X-ray flux, infrared fluxes at near, medium, and far beams (S12, S25, S60, S100) in the unit (Jy), radio fluxes at 1.4GHz (λ=21cm) & 5GHz (λ=6cm), an optical flux of OII at (λ=372.6nm) and ultraviolet fluxes at near (λ=177nm) & far (λ=153.9nm). The total apparent corrected B-magnitude m_B from the French website Lyon-Meudon Extragalactic Database (HYPERLEDA) was selected. The physical parameters (galaxies name, the morphology of starburst galaxies, z, m_B, S12, S25, S60, S100, S_{X-ray}, $S_{OII,}$ magnitudes of far ultraviolet (m-$_{FUV}$ (AB)) and near ultraviolet (m-$_{NUV}$ (AB)) and radio fluxes at ν=1.4GHz & ν=5GHz) of starburst galaxies are listed in Table (1).

Table 1: The data of starburst galaxies collected from NED, HYPERLEDA.

No.	Name	Morph.	z	S_{X-ray} (ergs/ s/cm^2)	S_{12} (Jy)	S_{25} (Jy)	S_{60} (Jy)	S_{100} (Jy)	S_{5GHz} (Jy)	$S_{1.4GHz}$ (Jy)	m_B	m-FUV (AB)	m-NUV (AB)
1	NGC6946	SAB(rs)cd	0.00013	3.21E-12	12.11	20.7	129.78	290.69	0.344	0.1883	8.23	10.425	9.741
2	NGC1614	SB(s)c pec	0.01594	6.50E-13	1.441	7.5	32.12	34.32	0.063	0.1382	12.71		
3	NGC2369	SB(s)a	0.01081	7.50E-14	0.74	2.2	20.35	38.31	0.035		12.13		
4	NGC3110	SB(rs)b pec	0.01686	9.70E-14	0.59	1.13	11.28	22.27	0.041	0.1288	12.34		
5	NGC3256	pec	0.00935	3.45E-12	3.57	15.69	102.63	114.31	0.319	0.659	11.29		
6	NGC3690	S pec	0.01041	4.80E-13	3.9	24.14	121.64	122.45	0.362	0.977	11.41	14.11	13.63
7	ESO320-G030	(R')SAB(r)a:	0.01078	5.80E-14	0.53	2.28	34.38	46.28	0.0321	0.0644	12.6		
8	NGC7130	Sa pec	0.01615	2.66E-13	0.58	2.16	16.71	25.89		0.1906	12.67	15.918	15.0098
9	IC860	S?	0.01291	1.23E-14	0.14	1.34	18.61	18.66	0.021	0.0313	14.14	21.01	18.35
10	NGC1569	IBm	-0.00035	1.93E-12	0.794	9.03	54.36	55.29	0.198	0.3619	8.31	15.38	14.82
11	NGC5135	SB(s)ab	0.01369	5.54E-13	0.63	2.401	16.86	30.97	0.107	0.2005	12.47	16.0224	15.1493
12	NGC5653	(R')SA(rs)b	0.0119	3.60E-15	0.64	1.37	10.57	23.03	0.031	0.05203	12.69	15.85	15.06
13	NGC5734	S0^0 pec edge-on	0.01375	7.30E-14	0.78	0.98	8.09	2.62E+01		0.0768	13.29	18.1375	17.0437
14	NGC5743	Sb:	0.01374	5.40E-14	0.59	0.75	5.21	2.28E+01		0.0567	12.85	16.518	15.9731
15	IC5179	SA(rs)bc	0.01141	1.27E-13	1.18	2.4	19.39	37.29	0.079	0.1697	12.03		
16	Zw049.057	Irr	0.01306	4.11E-15	0.05	0.95	21.89	31.53	0.03169	0.051	15.15	22.29	19.55

17	IC4734	(R')SB(s)ab pec:	0.01605	4.00E-14	0.38	1.33	14.04	25.31			13.42		
18	NGC7771	SB(s)a	0.01446	7.24E-13	1.23	2.9	20.93	44.85	0.0263	0.141	12.3	16.89	16.09
19	NGC7469	(R')SAB(rs)a	0.01627	3.90E-11	1.63	5.7	23.13	39.91	0.0616	0.178	12.48	14.87	14.04
20	NGC7679	SB0 pec:	0.01715	3.56E-13	0.498	1.12	7.4	10.71	0.00799	0.0558	13.02	15.42	15.29
21	NGC7769	(R)SA(rs)b	0.01405	3.09E-13	0.52	0.97	5.21	2.96E+01	0.00054	0.0599	11.55	15.34	14.93
22	mrk201	IBm pec	0.00834	2.10E-13	0.99	4.51	23.2	25.16	0.036	0.101	12.58	15.69	14.96
23	mrk529	S0^+ pec:	0.01184	2.03E-14	0.1184	0.2283	1.689	2.586	0.007	0.0116	14.55	17.0602	16.4672
24	mrk538	SB(s)b: pec	0.00933	5.77E-13	0.56	3.15	10.73	12.46	0.0141	0.0669	12.52	14.37	13.72
25	mrk545	SB(s)a	0.01523	5.71E-14	0.66	1.29	9.03	15.66	0.035	0.0735	12.51	16.01	15.4772
26	mrk732	cD pec	0.02925	4.00E-13	0.1611	2.55E-01	1.75	3.386	0.019	0.0422	13.74	17.4636	16.7661
27	mrk739	S?	0.02985	1.40E-11	0.1603	0.3093	1.26	2.408	0.009	0.0112	14.29	17.5615	16.6914
28	mrk789	compact	0.03144	6.42E-14	0.1457	0.6177	3.352	5.068	0.013	0.0355	14.63		
29	mrk841	E	0.03642	1.24E-11	0.1924	0.4726	0.4593	6.18E-01	0.00389	0.0148	13.71	15.3773	15.2851
30	mrk930	WR	0.0183	1.40E-14	7.88E-02	0.2317	1.245	2.15E+00	0.00272	0.0131		15.72	15.32
31	mrk1259	S0 pec?	0.00728	2.30E-13	0.941	4.881	14.7	2.77	0.0034	0.067	12.69	15.4871	14.8749
32	Mrk18	S?	0.01113	3.00E-14	0.1444	0.2522	2.157	2.97	0.0024	0.0303	13.78	16.86	16.8238
33	mrk0213	SB(s)a	0.01038	1.30E-12	0.2786	0.6134	3.936	6.006		0.0282	12.87		15.0446
34	mrk0190	SA(s)b?	0.00326	3.45E-14	0.26	0.47	3.07	5.79		0.0122	13.05	15.41	14.97

35	mrk0052	SB0^+(rs):	0.00714	8.40E-14	10.43	1.23	4.43	6.65	0.0427	0.0148	12.93	15.27	15.09
36	mrk0326	SAB(r)bc:	0.01187	3.68E-13	0.2318	0.7145	3.956	5.915		0.0173	13.3	16.24	15.92
37	mrk1066	(R)SB0^+(s)	0.01189	2.39E-13	0.46	2.35	11.01	12.48	0.02816	0.1	13.59		
38	NGC3077	I0 pec	0.00005	7.16E-14	0.76	1.88	15.9	26.53	0.022	0.029	10.2		
39	NGC4214	IAB(s)m	0.00097	4.00E-12	0.58	2.46	17.57	29.08	0.034	0.0016	9.91	11.5	11.28
40	NGC4449	IBm	0.00069	1.98E-12					0.136	0.2686	8.98	10.86	10.81
41	NGC5253	pec	0.00136	1.21E-13	2.72	12.07	30	30.08	0.09	0.0857	9.87	12.64	11.94
42	I Zw18	WR	0.00025	2.00E-14				0.0153	0.00114	0.00183	15.77	16.07	16.12
43	VII Zw403	pec	-0.00034	1.20E-13	7.98E-02	5.37E-02	0.3834	8.96E-01		0.0025	14.57	15.24	15.29
44	M82	I0 edge-on	0.0009	1.89E-14	71.55	332.63	1480.42	1373.69	0.024	6.4468	7.66	13.39	12.59
45	NGC1482	SA0^+ pec edge-on	0.00639	1.01E-13	1.55	4.68	33.36	46.73	0.125	0.34	12.89	17.7	16.33
46	NGC253	SAB(s)c	0.00081	3.50E-12	41.04	154.67	967.81	1288.15	2.08	2.9947	6.62	11.15	10.94
47	NGC3628	Sb pec edge-on	0.00282	1.64E-12	3.13	4.85	54.8	105.76	0.276	0.2917	9.15	14.31	13.63
48	NGC3079	SB(s)c edge-on	0.00369	2.45E-13	2.54	3.61	50.67	104.69	0.0448	0.865	9.97	14.02	13.59
49	NGC4631	SB(s)d edge-on	0.00203	1.38E-12	5.16	8.97	99.69	160.08	0.341	0.9816	7.99	11.76	11.49
50	Haro3	Sb? pec	0.00314	1.73E-13	0.27	0.97	5.17	6.746		0.0173	12.95	14.75	14.44

#	Name	Type											
51	Haro 9	SB(s)0/a pec:	0.00363	1.47E-15	1.62E-01	0.2843	2.634	4.47		0.0157	13.02	14.31	14.07
52	NGC 7552	(R')SB(s)ab	0.00536	8.74E-13	3.76	12.43	77.37	104.85	0.139	0.058	11.06	14.29	13.56
53	NGC 5236	SAB(s)c	0.00171	3.10E-12	21.46	43.57	265.84	524.09	0.648	2.445	7.5	10.62	10.04
54	Mrk1500	very compact	0.02985		7.84E-02	0.08856	0.4665	9.20E-01		0.0057	15.33	17.3444	17.0683
55	mrk1301	S0/a	0.00537						0.005	0.00315	14.18	17.98	16.88
56	N5350	SB(r)b	0.00775	3.72E-14	0.1411	0.327	2.22	8.76		0.00406	11.89	14.75	14.22
57	NGC1068	(R)SA(rs)b	0.00379	2.07E-11	39.84	87.57	196.37	257.37	0.664	4.85	9.47	12.79	12.22
58	mrk1308	S0	0.00382		0.08	0.25	1.04	1.35	0.016	0.0028	13.93		
59	mrk325	(R')SAc ? pec	0.01137	2.78E-13	0.14	0.52	4.98	6.66	0.015	0.0434	12.35	14.65	14.4
60	mrk1089	SB(s)m pec:	0.01341						0.035		14.76		
61	mrk1012	(R')SB(rs)a	0.01634		0.225	0.521	3.186	5.395	0.016	0.0147	13.77		
62	N1569	IBm	-0.00035	2.78E-12	1.24	9.03	54.36	55.29	0.278	0.3386	8.31	15.38	14.82
63	Mrk4	SB(s)dm:	0.0177		0.1403	0.2665	2.34	4.139	0.003	0.0146	13.77	20.0041	18.8654
64	N2782	SAB(rs)a pec	0.00853	5.40E-13	0.64	1.51	9.17	13.76	0.05	0.0344	12.1	14.82	14.38
65	mrk1087	S0 pec:	0.02781						0.014	0.0128	14.76		
66	N3351	SB(r)b	0.0026	3.33E-13	1.04	2.79	19.66	41.1		0.0436	10.14	13.5	12.97
67	N3504	(R)SAB(s)ab	0.00509	4.03E-13	1.11	4.03	21.43	34.05	0.098	0.292	11.44	14.29	13.68
68	N3888	SAB(rs)c	0.00799	1.79E-13	0.3621	0.4515	4.576	11.52	0.025	0.0318	12.47	14.99	14.53
69	N3994	SA(r)c pec?	0.01028	3.39E-13	0.32	0.46	4.98	10.31	0.052	0.01247	12.78	15.9562	15.4544
70	mrk0100	pec	0.01206		0.1079	0.1031	1.409	4.149		0.006	13.68		
71	mrk0140	compact	0.0055		6.84E-02	1.06E-01	0.3697	0.6304		0.001	14.72	16.61	16.36
72	N4449	IBm	0.00069	1.98E-12					0.136	0.0499	8.98	10.86	10.81
73	N4536	SAB(rs)bc	0.00603	5.90E-13	1.6	4.04	30.26	44.51	0.114	0.1943	10.27	13.279	13.19

74	mrk1344	S0 pec?	0.01057		0.178	0.5373	2.817	2.561	0.019	0.0299	13.84		
75	NGC6552	SB?	0.02649	4.90E-14	0.191	1.029	2.453	2.693	0.04	0.0343	14.07		
76	NGC3395	SAB(rs)cd pec:	0.00539	3.72E-13	0.28	0.72	6.79	13			11.83	13.46	13.16
77	NGC1961	SAB(rs)c	0.01312	2.77E-13	0.9	0.99	7.17	23.37	0.06	0.1771	10.97	15.25	14.67
78	UGC07282	Sb edge-on	0.00343	2.91E-15	1.26	1.5	11.6	41.19	0.4	0.139	11.19	16	15.23
79	UGC07520	SA(s)b: edge-on	0.00842	1.25E-12	0.9964	3.57	10.27	17.15	0.097	0.164	10.77	14.94	14.27
80	IC694	1	0.01038	2.54E-13							12.95		
81	IC4686	WR	0.01656	3.52E-14	0.94	2.96	16.08	28.55			14.31		
82	IC4687	Sb: pec	0.01734	7.70E-14	1.01	3.55	20.2	27.54			13.62	17.1484	16.482
83	MCG +04-48-002		0.0139	8.00E-14	0.52	1.09	9.93	12.5		0.0856	12.63		
84	mrk149	S?	0.00558		7.46E-02	0.1942	0.4077	0.6274	0.005		14.86	18.26	17.4155
85	mrk496	S0?	0.0293		0.26	1.24	6.48	9.41	0.02	0.0484	13.96	15.97	15.61
86	mrk220	pec	0.01666							0.0184	14.94		
87	mrk307	S	0.01853		0.2	0.24	1.82	4.14	0.01	0.0197	13.26	15.37	
88	mrk308	I0?	0.02389						0.005	0.0173	14.52	17.49	16.923
89	mrk316		0.0409	2.60E-12					0.006	0.0075	14.65	17.4842	17.1468
90	mrk332	S	0.00802		0.3598	0.6212	4.871	9.493	0.004	0.0365	12.57	15.4	14.96
91	mrk369	extremely compact	0.01381						0.012	0.0046	14.46	17.1648	16.9802
92	mrk373		0.01953		0.1028	0.3164	1.826	2.688	0.005	0.0101	14.65	18.4391	17.8085
93	mrk409	S0	0.00515		8.39E-02	1.18E-01	0.2288	0.607		0.003	14.25	16.7902	16.5524
94	mrk412		0.01499		9.74E-02	2.33E-01	0.5163	6.98E-01			14.52	16.6103	16.2673
95	mrk465	S?	0.00898			0.09017	0.3971	8.12E-01	0.005		14.86		
96	mrk489	S	0.03195		1.10E-01	2.20E-01	1.809	4.69	0.008	0.016	14.13	16.24	15.96

97	mrk684	S?	0.04497	1.50E-12	0.1099	0.1292	0.4338	0.7503	0.004		14.68	15.907	15.8888
98	mrk691	S?	0.011		0.2006	0.5308	3.909	7.743	0.018	0.0307	12.49	14.4	13.95
99	mrk708	SB?	0.00682		0.46	0.8	5.36	8.24	0.017	0.0334	13.22	16.06	15.48
100	mrk603	S0^-pec:	0.00808		0.5	2.28	13.06	15.41	0.00429		12.85	15.34	14.86
101	mrk575	(R')SB(s)a	0.01829		2.25E-01	0.4908	2.791	5.368	0.005	0.0161	13.45		
102	mrk602	SB(rs)bc	0.00951		0.1658	0.6249	3.687	5.602	0.011	0.0153	13.44		
103	mrk752	SB(rs)bc pec	0.02042		0.13	0.18	0.79	1.35	0.014	0.0088	14.13		
104	mrk799	SB(s)b	0.0099		0.5	1.94	10.1	20.34	0.004	0.0659	12.43	15.07	14.63
105	mrk809	S?	0.02559		2.10E-01	0.2114	1.986	3.392	0.004		13.99		
106	mrk781	SB(rs)bc	0.00944		0.1363	4.39E-01	1.896	4.029	0.011	0.0092	12.71	15.12	14.72
107	mrk769	Sa? pec	0.0057		0.34	1.08	8.53	12.43	0.021	0.0379	12.32	14.36	14.13
108	mrk1194	SB0	0.01491		0.34	0.84	7.16	13.78	0.01306	0.0427	13.1		
109	mrk710	SB(rs)ab	0.00486		0.16	0.44	2.95	4.41	0.006	0.0118	13.02	15.96	14.85
110	mrk711		0.01792		7.74E-02	0.3969	0.8092	0.749	0.00172	0.0029		18.5096	17.8728
111	mrk717	S?	0.02122		0.2233	0.7649	3.839	4.01	0.009	0.026	14.18	17.9982	17.113
112	mrk719	very compact	0.03203		1.46E-01	4.36E-01	1.164	1.76	0.012	0.00608	14.3	17.1962	16.7402
113	mrk759	SAB(rs)c	0.00724		0.2995	0.537	4.116	8.727	0.013	0.0319	12.37	14.34	13.99
114	mrk764	3	0.06614		1.37E-01	1.73E-01	0.421	0.95	0.006	0.006	14.47	18.0402	17.3423
115	mrk1134	I0:	0.01692		0.64	0.54	3.96	8.02	0.017	0.0249	14.02	16.81	16.32
116	mrk1093	(R')SB(rs)a pec	0.01487		0.33	1.35	9.56	12.76	0.027	0.0291	13.84		
117	NGC2366	IB(s)m	0.00034	2.39E-13	1.17E-01	0.699	3.513	4.68	0.001	0.117	10.52	12.78	12.71
118	NGC1808	(R)SAB(s)a	0.00334	1.45E-12	5.4	17	105.55	141.76	0.238	0.519	10.28	14.68	13.75
119	NGC2403	SAB(s)cd	0.00044	1.60E-15	2.82	6.29	41.47	148.49	0.0053	0.33	8.13	10.69	10.5
120	NGC4038	SB(s)m pec	0.00542	1.42E-12	2.92	7.11	46.88	85.69	0.246	0.2589	10.36	13.18	12.35
121	NGC4569	SAB(rs)ab	-0.00078	4.34E-14	1.27	2.06	9.8	26.56	0.004	0.157	9.49	14.456	13.54

122	NGC4670	SB(s)0/a pec:	0.00363	8.76E-16	1.62E-01	0.2843	2.634	4.47		0.0157	13.02	14.19	14.07
123	NGC4861	SB(s)m :	0.00279	7.42E-13				0.0063		0.01	12.04	13.62	13.65
124	NGC5055	SA(rs)c	0.00167	1.80E-14	5.35	6.36	40	139.82	0.116	0.456	8.89	12.55	12.03
125	NGC5457	SAB(rs)cd	0.00008	1.73E-15	6.2	11.78	88.04	52.84		0.75	8.29	10.05	9.88
126	NGC1705	SA0^- pec:	0.00211	1.30E-15	0.019	0.15	0.97	1.22			12.75	13.381	13.4
127	NGC1672	SB(s)b	0.00444	7.65E-13	2.47	5.25	41.21	77.92	0.107	0.722	10.15	15.2475	12.16
128	mrk357		0.05285		9.75E-02	1.71E-01	0.9565	0.9122		0.0076		16.2569	16.085
129	NGC2798	SB(s)a pec	0.00058	2.58E-14	0.76	3.2	19.29	29.69	0.036	0.082	12.5	16.44	15.64
130	NGC3310	SAB(r)bc pec	0.00331	1.09E-12	1.54	5.32	34.56	44.19	0.149	0.3642	11.15	12.67	12.18
131	NGC3448	I0	0.00045	3.81E-13	0.22	0.76	6.64	11.17	0.039	0.0525	11.55	14.4	13.99

Schmidt and Green defined the relationship between observed flux density and luminosity as [6]:

$$L(E_1, E_2) = 4\pi\, c(z)A^2(z)S(E_1, E_2) \tag{1}$$

for an energy band, E_1 to E_2, where $c(z)$=k-correction term, $A(z)$=luminosity distance term, and $S(E_1, E_2)$=observed flux density between E_1, E2 bands, and z=redshift. In astronomical ideas, redshift z is often used as a distance metric, and hence provides information about ages and temporal period [19]. The luminosity distance term A (z)and the k-correction term c (z) for power-law spectra with energy index and Friedman cosmology with $q_0 = 0.5$ are given by [6]:

$$c(z) = (1 + z)^{-(1+\alpha)} \tag{2}$$

$$A(z) = 2\left(\frac{c}{H_0}\right)[(1 + z) - (1 + z)^{0.5}] \tag{3}$$

Where α = spectral index at each electromagnetic spectrum, c =speed of light and its value are equal to $3*10^{10}$ cm/sec and H_0 =the Hubble constant, based on the (NED), we adopted the value $H_0= 67.8$ km s^{-1} Mpc^{-1}, $\Omega m = 0.3$(Omega Matter), and $\Omega_\Lambda = 0.7$(Omega vacuum) [20][21]. To obtain the main luminosity equation by substituting the values of c (z) and A (z) into the general luminosity equation as:

$$L(E1, E2)=4\pi\left(\frac{c}{H_0}\right)^2 (1+z)^{-(1+\alpha)}\left[2[(1 + Z) - (1 + Z)]^{0.5}\right]^2 S(E1, E2) \tag{4}$$

To determine all the luminosities from X-ray to radio emission, "Eq. (4)" was employed.

2.1 X-ray Luminosity (L_{X-ray}):

In the X-ray range, the energy index is $\alpha_x = -1.02$ for active galactic nuclei starburst galaxies [7], and the flux density S_{X-ray} in (erg s^{-1} cm^{-2}), as a result, the X-ray luminosity is acquired by the following equation:

$$L_{X-ray}=4\pi\left(\frac{c}{H_0}\right)^2 (1+z)^{-(1-1.02)} \left[2[(1 + Z) - (1 + Z)^{0.5}]\right]^2 S_{X-ray} \tag{5}$$

Where L_{X-ray} = X-ray luminosity in a unit (erg/s).

2.2 The optical luminosity (L_{opt}):

The optical band monochromatic fluxes have been computed at 440 nm using the relationship [22]:

$$"S_{B(440nm)} = 3.63 \times 10^{-20} \times 10^{\frac{-m_B}{2.5}} \qquad (\text{erg cm}^{-2} \text{ s}^{-1} \text{ Hz}^{-1})" \qquad (6)$$

Where m_B= blue magnitude at 0.44μm (4400A^0) blue band. For the optical band, the spectral index is α_{opt}=-0.5 [7].

$$L_{opt} = 4\pi \left(\frac{c}{H_0}\right)^2 (1+z)^{-(1-0.5)} \left[2[(1+Z) - (1+Z)]^{0.5}\right]^2 S_{opt} \qquad (7)$$

$$L_{OII} = 4\pi \left(\frac{c}{H_0}\right)^2 (1+z)^{-(1-0.5)} \left[2[(1+Z) - (1+Z)]^{0.5}\right]^2 S_{OII} \qquad (8)$$

Where S_{OII} =flux density of OII line emission at λ= 372.7nm in a unit (erg s^{-1} cm^{-2}).

2.3 Infrared Luminosity (L_{IR}):

IRAS 12, 25, 60, and 100 microns (μm) band fluxes were used to calculate the IR and FIR fluxes from the equations [6]:

$$S_{FIR(42.5-122.5 \text{ micron})} = 1.26 \times 10^{-11} (2.58S_{60} + S_{100}) [erg \, cm^{-2} \, s^{-1}] \qquad (9)$$

$$S_{IR} = 1.8 \times 10^{-14} (13.4S_{12} + 5.16S_{25} + 2.58S_{60} + S_{100}) [erg \, cm^{-2} \, s^{-1}] \qquad (10)$$

Where S_{12}, S_{25}, $S_{60,}$ and S_{100} are given in Jy at the band interval (8-1000 micron). For the infrared band of starburst galaxies, the spectral index is $\alpha_{IR, FIR}$ = - 0.5 [6].

$$L_{FIR} = 4\pi(\frac{c}{H_0})^2 (1+z)^{-(1-0.5)} \left[2[(1+Z) - (1+Z)]^{0.5}\right]^2 S_{FIR} \qquad (11)$$

$$L_{IR} = 4\pi(\frac{c}{H_0})^2 (1+z)^{-(1-0.5)} \left[2[(1+Z) - (1+Z)]^{0.5}\right]^2 S_{IR} \qquad (12)$$

Both far-infrared in the region (40-100)μm L_{FIR} and total infrared between 8-1000μm L_{IR} luminosities are given in (erg/s).

2.4 Radio Luminosity (L_{radio}):

For the radio continuum, the spectral index is α_R=-0.8 [7]. Units in [erg cm^{-2} s^{-1} Hz^{-1}] were used to compute the radio flux densities at (υ=5GHz & υ=1.4GHz) or (λ=6cm & λ=21cm).

$$L_{1.4GHz} = 4\pi(\frac{c}{H_0})^2 (1+z)^{-(1-0.8)} \left[2[(1+Z) - (1+Z)]^{0.5}\right]^2 S_{1.4GHz} \qquad (13)$$

$$L_{5GHz} = 4\pi(\frac{c}{H_0})^2 (1+z)^{-(1-0.8)} \left[2[(1+Z) - (1+Z)]^{0.5}\right]^2 S_{5GHz} \qquad (14)$$

Where $S_{1.4GHz, 5GHz}$ =$S_{1.4GHz, 5GHz}$ (Jy) × 10^{-23} measured by (erg s^{-1} cm^{-2} Hz^{-1}), 1Jy=10^{-26}w m^{-2}Hz^{-1}, or 1Jy=10^{-23}erg s^{-1} cm^{-2} Hz^{-1} in units systm (c.g.s) [7].

2.5 Ultraviolet Luminosities (L_{FUV}, L_{NUV}):

The magnitude of far-ultraviolet at λ=151.6nm m_{FUV} is calculated [18]:

$$m_{FUV} = 23.9 - 2.5 Log S_{FUV} (mJy) \qquad (15)$$

We derive the relation between the far-ultraviolet flux density as follows:

$$S_{FUV} = 10^{-26} \times 10^{(-m_{FUV} + 23.9)/2.5} [erg \, s^{-1} \, cm^{-2} \, Hz^{-1}] \qquad (16)$$

Where m_{FUV} = magnitude of far-ultraviolet at 151.6nm in (mJy), and for near-ultraviolet, at λ=177nm (1770A^0) the equation of flux density is:

$$S_{NUV} = 10^{23} \times S_{NUV}(erg\ s^{-1}\ cm^{-2}\ Hz^{-1}) \qquad [Jy] \qquad (17)$$

The spectral index UV band for active starburst galaxies is α_{UV}=-0.9 [18].

$$"L_{FUV} = 4\pi(\frac{c}{H_0})^2 (1+z)^{-(1-0.9)} \left[2[(1+Z)-(1+Z)]^{0.5}\right]^2 S_{FUV}" (18)$$

$$"L_{NUV} = 4\pi(\frac{c}{H_0})^2 (1+z)^{-(1-0.9)} \left[2[(1+Z)-(1+Z)]^{0.5}\right]^2 S_{NUV}" (19)$$

Where far-to-near luminosities L_{FUV}, and L_{NUV} are given in unit (erg s^{-1} Hz^{-1}).

3.   Calculations, results and discussion.

We present the results of statistical analysis in this paper by using statistical software (statistic-win-program) application to see if there is a luminosity correlation between multiple bands. The statistical program is frequently used to analyze and evaluate numerous associations between variables, as well as to determine whether or not there is regression strength between the two variables' characteristics. The linear partial correlation coefficient (R) values are in the range of [+1,-1]. If the regression value is ±1, the two components are perfectly linked. Even so, when the measurement of regression correlation (R) is zero or close to zero, there is a weak regression correlation between the two components. The relationships between logarithms of luminosities of wavelength bands from radio to X-rays when using multiple regression analysis on our sample of 131 starburst galaxies were studied. The partial correlation coefficient (R), significance levels (P), and the slopes were calculated for each relationship.

The relationship between X-ray luminosity as a dependent variable and radio luminosity at (5GHz & 1.4 GHz) as independent variables. From the results of the statistical analysis, we find that there is a good correlation between X-ray luminosity and radio luminosity at 1.4GHz where the partial correlation coefficient is (R=0.53) and slope (0.6±0.12) for N=81, where N is the correct sample number under test (see Figures 1a, 1b).
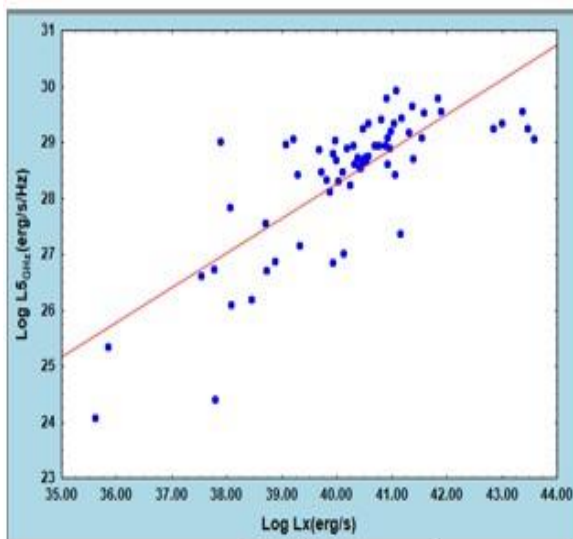
Figure 1-(a) The relationship between (Log L$_{X-ray}$) and (Log L$_{5GHz}$).
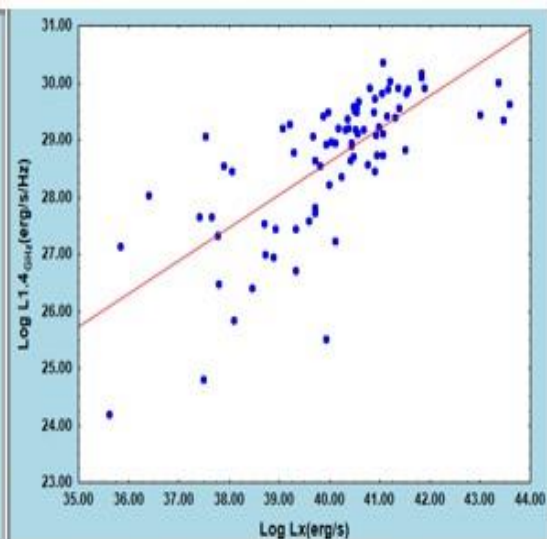
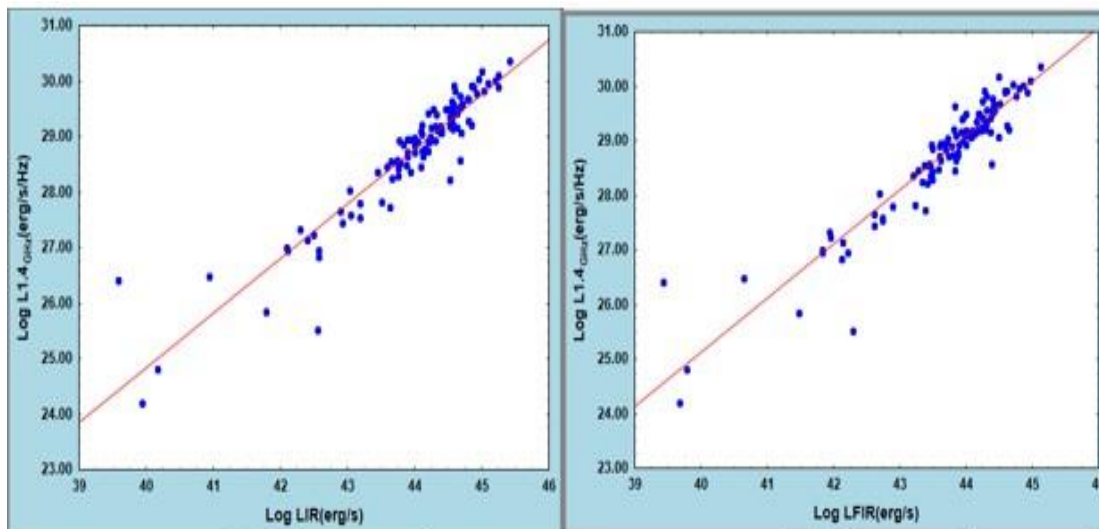**Figure 1-**(b) The relationship between (Log L$_{X-ray}$) and (Log L$_{1.4GHz}$).

There is also a significant correlation between X-ray luminosity and radio luminosity at 5GHz with a good partial correlation coefficient (R≈ 0.65) and slope (0.77±0.11) for N=68. There are good positive relationships between radio luminosity at (1.4GHz, 5GHz) with infrared and far-infrared luminosities. (Log $L_{1.4GHz}$ α log $L_{FIR}^{0.89±0.04}$ α Log $L_{IR}^{0.9±0.03}$) with a very strong correlation equal to R≈0.9 and (Log L_{5GHz} α Log $L_{FIR}^{0.79±0.05}$ α Log $L_{IR}^{0.81±0.05}$) with a strong correlation R≈0.8 both with very higher probability level p≈10^{-7}, for N=108 (see Figures 2a, 2b, 2c and 2d).
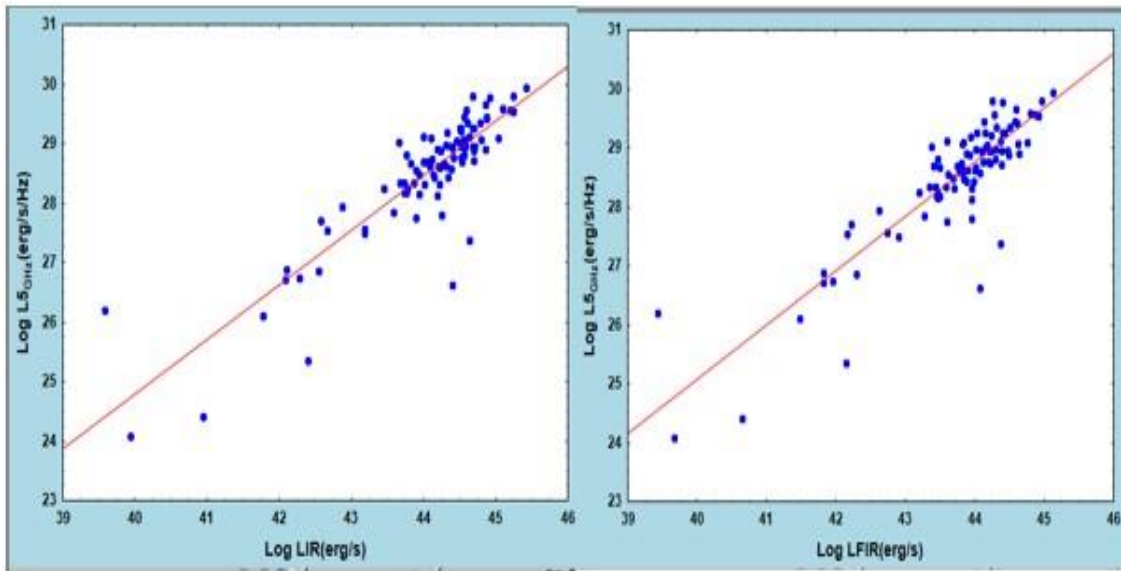
Figure 2- (a) The relationship between (Log L_{5GHz}) and (Log L_{IR}).

Figure 2- (b) The relationship between (Log L_{5GHz}) and (Log L_{FIR}).

Figure 2- (c) The relationship between (Log $L_{1.4GHz}$) and (Log L_{IR}).

Figure 2- (d) The relationship between (Log $L_{1.4GHz}$) and (Log L_{FIR}).

One of the closest and most correlations known among the global features of local star formation and starburst galaxies is the link between far-infrared (FIR) and radio emission. This tight global correlation was unexpected at the time of this significant discovery because the

radio and FIR emissions were thought to be caused by distinctly different physical processes. Namely, the radio continuum emission is primarily caused by synchrotron emissions from relativistic cosmic-ray electrons gyrating around galactic magnetic fields, whereas the FIR emission is primarily caused by thermal emissions from dust grains submerged in an intense ultraviolet (UV) radiation field. The current qualitative physical explanation for such a global correlation is that FIR is caused by dust grain absorption of UV photons emitted by nearby young massive stars, whereas sources of relativistic cosmic-ray electrons are primarily associated with magneto hydro dynamic (MHD) shocks of massive stellar winds or supernova explosions – the primary source of UV radiations that heat interstellar dust grains, and these results agree with [23].

Moreover, the link between radio luminosity at (5GHz) and optical luminosity (Log L_{5GHz} α Log $L_{opt}^{0.43\pm0.10}$) is weaker than the link between radio luminosity at (1.4GHz) and optical luminosity (Log $L_{1.4GHz}$ α Log $L_{opt}^{0.69\pm0.1}$) with correlation equal to R=0.39 & R=0.64 respectively both with very higher probability level p≈10^{-7}, for N=117 (Figures 3a, 3b). Since radio emission from a starburst originates in H II regions and supernovae, it is mostly unaffected by extinction. Optical emission-line ratios can be used to determine the major energy source inside a galaxy since they represent local excitation conditions, with the caveat that optical wavelengths may not notice a substantially veiled starburst or AGN. The radiation of plasma accreting onto supermassive black holes dominates the optical emission of quasars, or active galactic nuclei (AGN), while plasma outflowing from black hole/accretion disk complexes dominates the radio emission. As a result, separate but complementary information about the cosmic development of AGNs and their relationship to structure formation in the universe may be acquired in both photon energy ranges. This correlation could be a result of the flux restrictions and the large range of redshifts. Furthermore, it could be a result of the stellar population and these agree with the results of [24].
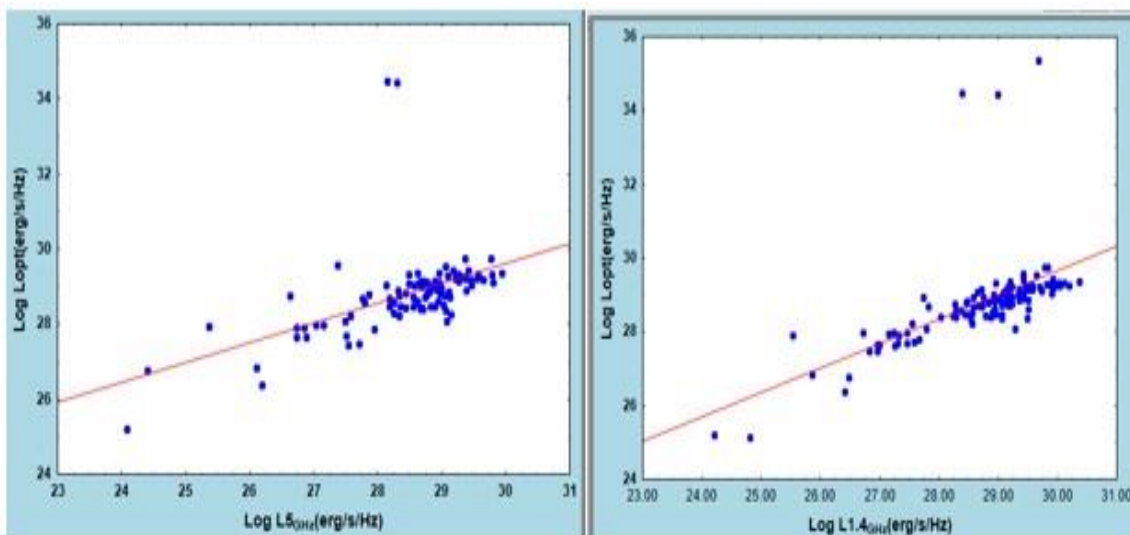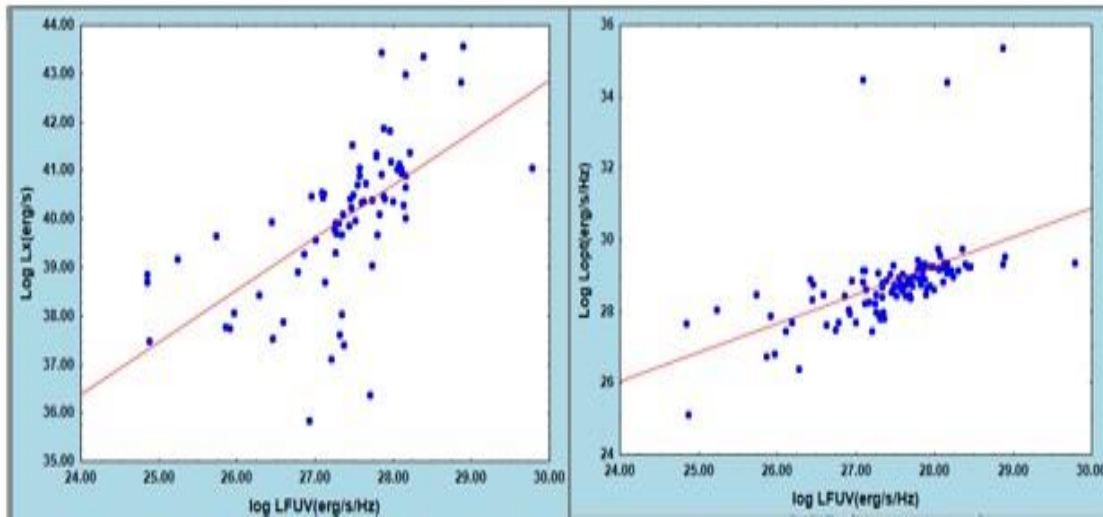

Figure 3: (a) The relationship between (Log L_{5GHz}) and (Log L_{opt}).　　**Figure 3:** (b) The relationship between (Log $L_{1.4GHz}$) and (Log L_{opt}).

There are weak relationships between far-ultraviolet as a dependent variable and (L_{OII}, L_{X-ray}, L_{opt}) as independent variables. The slopes of the relationships are not linear but rather flat (Log L_{FUV} α Log $L_{OII}^{0.34\pm0.12}$ α Log $L_{X-ray}^{0.35\pm0.08}$ α Log $L_{opt}^{0.37\pm0.09}$) with a weak correlation equal to R≈0.348, R≈0.43, and R≈0.37 respectively, and probability level P≈9×10^{-3}, P≈10^{-4} & P≈10^{-}

[4], for N= 58, N=54 & N=102 respectively (as shown in Figures 4a, 4b, and 4c). The weak correlation between these relationships may be the result of statistical analysis, which may hide this correlation due to the strong correlation between X-ray & radio/ radio& FIR/ radio& optical/ X-ray &FIR emission.

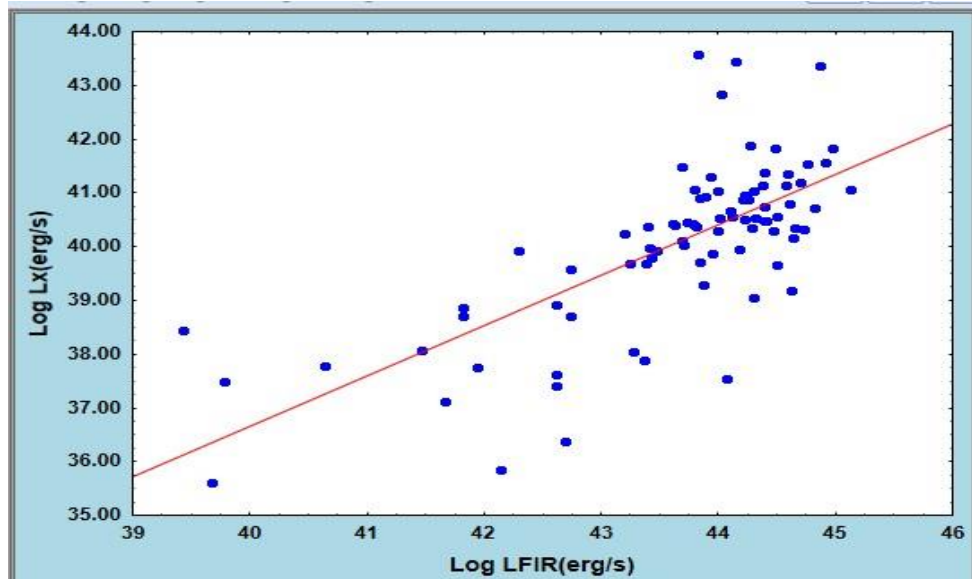**Figure 4-**(a) The relationship between (Log L_{X-ray}) and (Log L_{FUV}).

Figure 4-(b) The relationship between (Log L_{opt}) and (Log L_{FUV}).
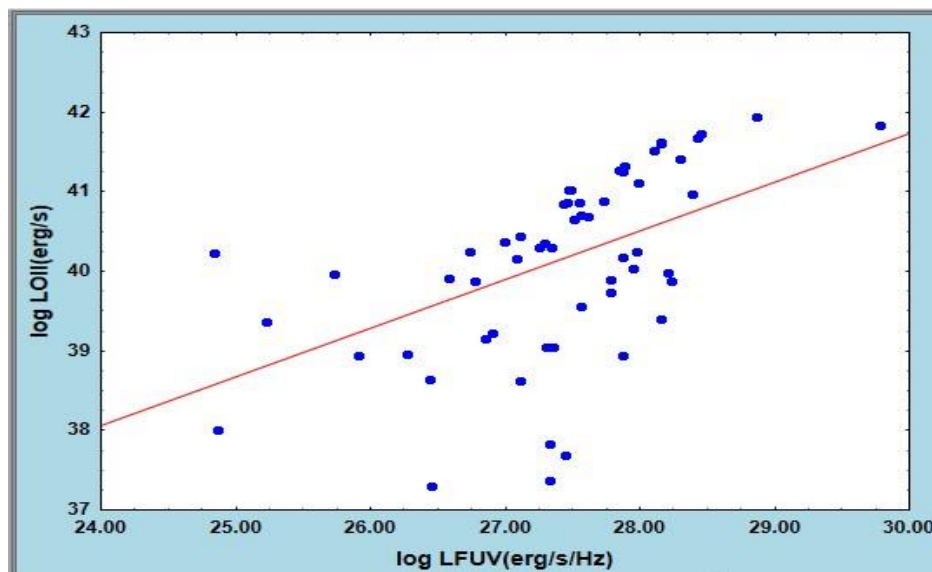
Figure 4: (c) The relationship between (Log L_{OII}) and (Log L_{FUV})

There is a good positive relationship between L_{X-ray} and L_{FIR} with a good partial correlation equal to R≈0.57, slope (0.45±0.07), and high probability level p≈10^{-7}, for N=84. An empirical correlation between the FIR and X-ray global luminosities from the young objects (e.g. HMXBs) has been reported in star-forming galaxies and the correlation is naturally interpreted in terms of star formation activities in galaxies, which in turn implies a correlation between X-ray luminosity and star formation rate (SFR). David, Jones & Forman (1992) derived a linear relationship between the logarithms of X-ray (0.5–4.5) keV and FIR luminosities in the normal and starburst galaxies using the X-ray data of the EINSTEIN satellite and suggested a two-component model fit this correlation[25]. The existence of a strong link between global far-infrared (FIR) and radio continuum (1.4 and 4.8 GHz) fluxes/luminosities from star-forming

galaxies has been known for two decades, which may be explained by tremendous star formation processes in these galaxies. As a result, a link between X-ray and FIR/radio global luminosities of galaxies may exist.

Figure 5: The relationship between Log $L_{X\text{-ray}}$ and Log L_{FIR}

In addition, we find a strong significant correlation between L_{NUV} & $L_{1.4GHz}$ and between L_{NUV} & L_{FIR}. The partial correlation between L_{NUV} & $L_{1.4GHz}$ is equal to R≈0.631 and slope is (0.63±0.08), and for the relationship between L_{NUV} & L_{FIR} the slope is (0.68±0.08) and the partial correlation is equal to R≈0.64 with N=95 for both. This is why infrared measurements of starbursts are so important: infrared luminosities are significantly less susceptible to extinction. Two spectral "features" that are intrinsic to the same starburst are the infrared emission and the ultraviolet monochromatic continuum. The infrared is generated by photons from the continuing starburst in the photodissociation area immediately surrounding it. This infrared emission is unique to the photodissociation zone and occurs whether or not the starburst is obscured by dust. It is as much a part of the starburst as hot star radiation or emission lines from the HII region. The same obscuring dust in the surrounding cold molecular cloud affects both infrared and ultraviolet characteristics; however, the UV feature suffers significant extinction while the infrared feature suffers little extinction.
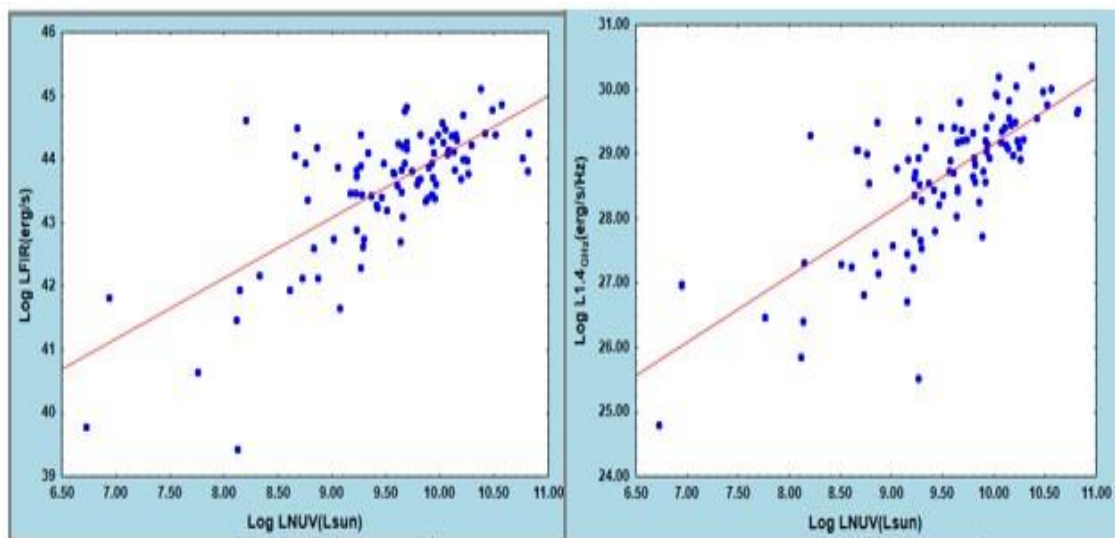

Figure 6:(a) The relationship between   **Figure 6:**(b) The relationship between

(Log L_{FIR}) and (Log L_{NUV}).   (Log $L_{1.4GHz}$) and (Log L_{NUV}).

We furthermore find that there is no strong correlation between the far-infrared and optical luminosities. The correlation is equal to R≈0.46 with slope (0.44±0.08) for N=120. A significant dispersion due to the uncorrelated temporal variability of star formation and accretion activity may overshadow a correlation between the optical and FIR luminosities.
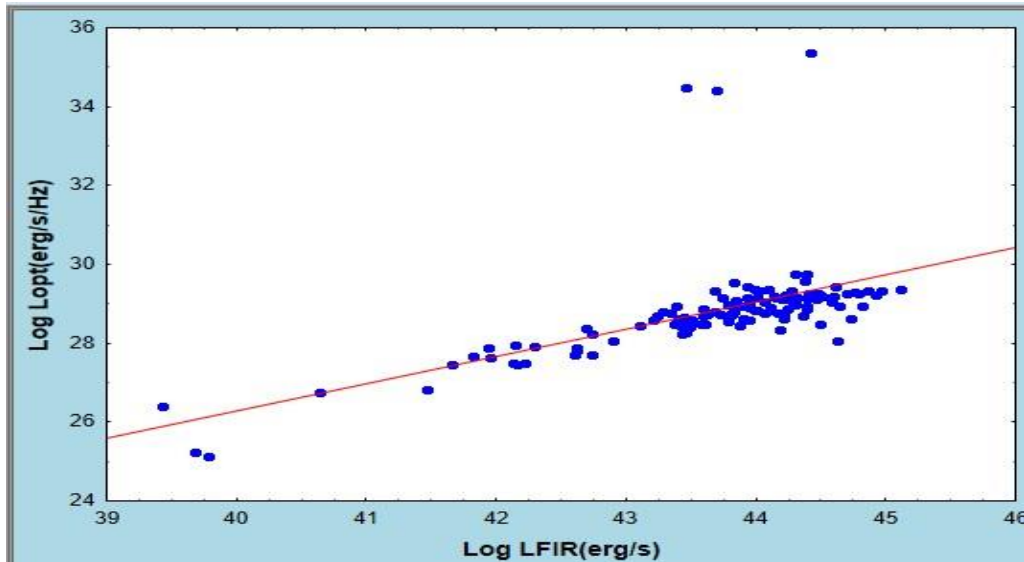
Figure 7: The relation between (Log L_{FIR}) and (Log L_{opt}).

4. Conclusion

Various correlations exist between the FIR, radio, and X-ray luminosities of starburst. From the results of the statistical analysis, we have found that there is a linear relationship between L_{X-ray} and L_{FIR} for star-forming regions, with a flat slope (0.45±0.07) and good partial correlation equal to R≈0.57. This correlation is naturally interpreted in terms of star formation activities in galaxies, which in turn implies a correlation between X-ray luminosity and star formation rate (SFR). There are good positive relationships between radio luminosity at (1.4GHz, 5GHz) with far-infrared luminosity, with steep slopes (Log $L_{1.4GHz}$ α log $L_{FIR}^{0.89\pm0.04}$) & (Log L_{5GHz} α Log $L_{FIR}^{0.79\pm0.05}$). The current qualitative physical explanation for such a global correlation is that FIR emission is primarily caused by dust grain absorption of UV photons emitted by nearby young massive stars, whereas sources of relativistic cosmic-ray electrons are primarily associated with magnetohydrodynamic (MHD) shocks of massive stellar winds or supernova explosions.

5. ACKNOWLEDGMENT

References
[1] R.M.G. Delgado, M.L.G. Vargas, J. Goldader, C. Leitherer, and A. Pasquali, " Multiwavelength study of the starburst galaxy NGC 7714. I: Ultraviolet-Optical spectroscopy," *The Astrophysical Journal*, vol. 513, pp. 707-719, 1999.
[2] G. Delgado, M. Rosa, "The stellar population and the evolutionary state of HII regions and starburst galaxies," *New Astronomy Reviews*, vol. 44, pp. 221-228, 2000.
[3] Th. Boller, E.J.A. Meurs, W. Brinkmann, H. Fink, U. Zimmermann, H.M. Adorf, "ROSAT ALL Sky Survey observations of IRAS galaxies," *Astronomy & Astrophysics*, vol. 261, pp. 57-77, 1992.
[4] T. Isobe and E.D. feigelson, Astrophys, J.Suppl. vol.79, p. 197, 1992.

[5]   J.H. Huang, Q.S. Gu, H.J. Su, T.G. Hawarden, X.H. Liao, and G.X. Wu, "The bae enhanced star-formation activities in spiral galaxies," *Astronomy &Astrophysics*, vol. 313, pp. 13-24, 1996.

[6]   R.A. kandalyan and H.M.K. Al-Naimi, "Broad-band radio to x-ray properties of Seyfert galaxies," *Astrophysics*, vol. 45, p. 3, 2002.

[7]   M. N. Al Najm, Y.E. Rashed, and H.H. AL-Dahlaky, "Spectral Multi-Wavelength Properties of an RBSC-NVSS Observation for a Sample of Active Galaxies," *Indian Journal of Natural Sciences*, vol. 1.9, no. 51, 2018.

[8]   Z. Adnan and A. K. Ahmed, "Photometric investigations of NGC 2577and NGC 4310LenticularGalaxies," *Iraqi Journal of Science*, vol. 59, pp. 1129-1138, 2018.

[9]   M. Liao, M. Gu, M. Zhou, and L. Chen, "The X-ray emission in young radio AGNs," *Astronomical Observatory, Chinese Academy of Sciences*, vol. 000, pp. 1-15, 2020.

[10] M.P. Santaella, A.A. Herrero, M..S. Lleo, L. Colina, E.J. Bail´on, "The X-ray emission of local luminous infrared galaxies," *Astronomy & Astrophysics*, vol. 535, 2011.

[11] M. D. Bicay, G. Kojoian, J. Seal, M. A. Malkan, "A MULTIFREQUENCY RADIO CONTINUUM AND IRAS FAINT SOURCE SURVEY OF MARRARIAN GALAXIES," *The Astrophysical Journal Supplement Series*, vol. 98, pp. 369-440, 1995.

[12] J.M. Mazzarella, V.A. Balzano, "A CATALOG OF MARKARIAN GALAXIES," *The Astrophysical Journal Supplement Series*, vol. 62, pp. 751-819, 1986.

[13] J. Ott, F. Walter, and E. Brinks, "A Chandra X-ray survey of nearby dwarf starburst galaxies – I. Data reduction and results," *Mon. Not. R. Astron. Soc*, vol. 358, p. 1423–1452, 2005.

[14] L. A. Sargsyan and D.W. Weedman, "STAR FORMATION RATES FOR STARBURST GALAXIES FROM ULTRAVIOLET, INFRARED, AND RADIO LUMINOSITIES," *The Astrophysical Journal*, vol. 701, p. 1398–1414, 2009.

[15] C. J. Latimer, A.E. Reines, R.M. Plotkin, T.D. Russell, and J. J. Condon, "An X-Ray + Radio Search for Massive Black Holes in Blue Compact Dwarf Galaxies", *The Astrophysical Journal*, vol. 884:78, p. 12, 2019.

[16] D. K. Strickland, T.M. Heckman, E. J.M. Colbert, C.G. Hoopes, and K. A. Weaver, " A high spatial resolution X-ray and Hα study of hot gas in the halos of star-forming disk galaxies. I. Spatial and spectral properties of the diffuse X-ray emission", *The Astrophysical Journal supplement series*, vol. 151, pp. 193-236, 2004.

[17] W.C. Keel, and E.T.M. Van Soest, " Pairing properties of Markarian starburst galaxies", *Astronomy and astrophysics*, vol. 94, pp. 553-568, 1992.

[18] A.L. Kinney, R.C. Bohlin, D. Calzetti, N. Panagia, and F.G. Rosemary, "Ultraviolet spectra of star-forming galaxies," *Astrophysical Journal Supplement*, vol. 86, pp. 5-93, 1993.

[19] H.A. Abd Al-Lateef and H.S. Mahdi, " The Dependence of The Gravitational Lensing Properties on The Lens And Source Redshifts", *Iraqi Journal of Science*, vol. 63, pp. 866-876, 2022.

[20] S. H. Kareem, Y.E. Rashed, " Studying the Correlation between Supermassive Black Holes and Star Formation Rate for Samples of Seyfert Galaxies (Type 1 and 2*)", Iraqi Journal of Physics*, vol. 19, pp.52-65, 2021.

[21] D.K. Abood, M.N. Al-Najm, "Investigation of the characteristics of CO (1-0) Line Integrated Emission Intensity in Extragalactic Spirals", *Iraqi Journal of Science*, vol. 63, pp. pp: 1376-1394,, 2022.

[22] Y. E. Rashed, M.N. Al-Najm, " Studying the Flux Density of Bright Active Galaxies at Different Spectral Bands", *Baghdad Science Journal*, vol. 16, 2019.

[23] Y.Q. Lou, and F.Y. Bian, "Correlations among multiwavelength luminosities of star-forming galaxies", *Mon. Not. R. Astron. Soc*. Vol.358, p.1231–1239, 2005.

[24] J. Singal, V. Petrosian, A. Lawrence, "ON THE RADIO AND OPTICAL LUMINOSITY EVOLUTION OF QUASARS", *The Astrophysical Journal*, vol. 743:104, p. 13pp, 2011.

[25] L.P. David, C. Jones, W. Forman, "X-ray properties of bright far-infrared galaxies", *Astronomical Journal*, vol. 388, p. 82, 1992.